PRAMANA
— journal of
physics

Vol. 65, No. 5
November 2005
pp. 855–862

Iron oxide nanoparticles stabilized inside highly ordered mesoporous silica

A BHAUMIK[1,*], S SAMANTA[1] and N K MAL[2]
[1]Department of Materials Science, Indian Association for the Cultivation of Science, Jadavpur, Kolkata 700 032, India
[2]Dynamic Materials Research Group, National Institute of Advance Science & Technology (AIST), Kansai Center, 1-8-31, Osaka 563-8577, Japan
*Corresponding author. E-mail: msab@mahendra.iacs.res.in

Abstract. Nanosized iron oxide, a moderately large band-gap semiconductor and an essential component of optoelectrical and magnetic devices, has been prepared successfully inside the restricted internal pores of mesoporous silica material through *in-situ* reduction during impregnation. The samples were characterized by powder XRD, TEM, SEM/EDS, N_2 adsorption, FT-IR and UV–visible spectroscopies. Characterization data indicated well-dispersed isolated nanoclusters of $(Fe_2O_3)_n$, within the internal surface of 2D-hexagonal mesoporous silica structure. No occluded Fe/Fe_2O_3 crystallites were observed at the external surface of the mesoporous silica nanocomposites. Inorganic mesoporous host, such as hydrophilic silica in the pore walls, directs a physical constraint necessary to prevent the creation of large Fe_2O_3 agglomerates and enables the formation of nanosized Fe_2O_3 particles inside the mesopore.

Keywords. Mesoporous MCM-41; nanomaterials; iron oxide; impregnation.

PACS Nos 81.05.Rm; 81.07.Bc; 81.16.Be; 82.35.Np

1. Introduction

Developments in the field of uniform nanometer sized particles have been studied extensively in recent times because of their technological and fundamental scientific importance [1]. These nanomaterials exhibit very interesting electrical, optical, magnetic, chemical and related surface properties, which is entirely different [2] from the respective bulk materials. The fabrication of low valent iron nanoparticles is also very important for their potential applications in wastewater cleanup process [3]. Such magnetic nanomaterials could also find applications in refrigeration systems, medical imaging, drug targeting and other biological applications [4] and catalysis [5]. The syntheses of several uniform-sized magnetic metal nanoparticles as well as metal oxides have been reported [6]. Mesoporous silica [7] with ordered or disordered channel structures which possesses uniform mesopores and exceptionally high surface area and thermal stability could be an ideal host for the synthesis of such nanostructured materials. High silanol density at the surface of

these materials helps to anchor the inorganic metal oxide/phosphate to be selectively deposited on its surface [8]. However, relatively little work has been done on the fabrication of magnetic metal oxide nanoparticles [9] and controlling their size using a rigid host [10–15]. On the other hand, many magnetic oxide nanoparticles have been synthesized in recent times by using microemulsion and other methods [16]. CdS nanoparticles prepared in reverse micellar system was incorporated into thiol-modified MCM-41 and the resulting CdS-FM41 composite showed photocatalytic activity for H_2 generation from water [17]. However, particle size uniformity of these nanomaterials is comparatively poor. Here we report the synthesis of nanosized particles of iron oxide through *in-situ* reduction using dispersed fine particles of MCM-41 in a homogeneous aqueous solution of iron (III) chloride. Magnesium powder was used as reducing agent under constant stirring at room temperature to complete the impregnation process.

2. Experimental

Highly ordered 2D hexagonal mesoporous pure silica MCM-41 was used as host in this post-synthesis impregnation method. Tetraethylorthosilicate (TEOS, E-Merck) was used as the silica source for the synthesis of silicious MCM-41. Cationic surfactant octadecyltrimethylammonium bromide (ODTMAB, TCI) was used as structure directing agent and NaOH (Loba Chemie) was used to maintain the pH of the medium. For the synthesis of 2D-hexagonal mesoporous MCM-41 material, TEOS was allowed to homogenize with an aqueous solution of ODTMAB. The aqueous solution of ODTMAB was prepared by dissolving it in deionized water. Then aqueous NaOH solution was added to it until pH rose to *ca.* 10. The final mixture was vigorously stirred for 1 h and then autoclaved at 353 K for two days. The molar ratio of various constituents of the hydrothermal gel was

$$SiO_2 : ODTMAB : NaOH : H_2O = 1 : 0.5 : 0.5 : 90.$$

After the hydrothermal treatment the solid products were filtered, washed with water and dried in air. Then it was calcined at 823 K to remove the template ODTMAB. This mesoporous support material (sample 1) with uniform nanopore opening was then dispersed in a homogeneous aqueous solution of iron (III) chloride. This was followed by the addition of magnesium powder to the mixture under constant stirring at room temperature. This mixture was aged under stirring condition for 2 h at room temperature. Three different iron-loaded samples were prepared in this Mg reduction method using 0.5, 0.8 and 1 M aqueous $FeCl_3$ solutions. These samples were designated as 2, 3 and 4 respectively. We have carried out other synthesis techniques for the preparation of iron oxide nanocomposites using impregnation of iron complexes of oxalic acid and acetyl acetone in mesoporous silica. However, loading of iron observed was very poor when compared to samples 2–4. Reference iron oxide samples were prepared following standard literature procedure [18]. Powder X-ray diffraction patterns of different as-synthesized and calcined samples were obtained with a Seifert XRD 3000P diffractometer using Cu K_α ($\lambda = 1.5404$ Å) radiation. For transmission electron microscopy measurement Hitachi H-9000NA instrument operating at 300 kV was used. N_2 adsorption measurements were carried out using a BELSORP 28SA at 77 K. Prior to N_2 adsorption,

samples were degassed for 2 h at 323 K. UV–visible diffuse reflectance spectrum was recorded in a Shimadzu UV 2401PC using $BaSO_4$ as background standard. FT-IR spectra of different samples were recorded in a Nicolet MAGNA-IR 750 Spectrometer Series II. Philips Xl-30/FEG, XL-serial scanning electron microscope with an EDS (New XL-30) attachment was used for the determination of morphology and surface chemical composition. Bulk chemical analyses of various samples were performed using a Perkin-Elmer AAS 3310 atomic absorption spectroscopy.

3. Results and discussion

We have prepared the iron oxide loaded MCM-41, optimized its iron-loading keeping the mesophase unperturbed and identified the nature of iron oxide species present in these mesoporous material. Physico-chemical properties of various iron oxide/silica nanocomposites synthesized in this study are given in table 1. Chemical analysis of these composite materials after calcination revealed the absence of any organic impurities. Iron loading on various mesoporous samples are given in table 1. Beyond 3% loading limit of iron resulted in disordered porous structures (sample 4, 1 M $FeCl_3$ solution was used in the reduction reaction). Typical XRD pattern of the pure mesoporous MCM-41 host (sample 1) is shown in figure 1, curve a. The other three curves b, c and d of figure 1 correspond to samples 2, 3 and 4, respectively, with 2.7 and 2.95 and 3.4 wt% iron-loaded MCM-41. As seen from figure 1, XRD patterns before and after the iron loading indicated progressive decrease in the ordering of mesostructures with the increase in strength of $FeCl_3$ solutions. Partial decrease in ordering could be attributed to the Mg/$FeCl_3$ treatment under aqueous acidic condition. High angle reflections observed for sample 2 (inset of figure 1) matches well with the crystalline α-Fe_2O_3 phase [19] together with the contribution due to the presence of amorphous silica (mostly in low 2θ diffraction angles). In figure 2 the TEM image of the sample after impregnation is shown. The existence of hexagonal arrangement of uniform mesopores is very clear. Change in contrast between the inorganic pore wall and iron oxide inside the channel may be an indication of the presence of iron oxide particles inside the mesoporous channels in the form of clusters. Uniform morphology of the composite material was observed throughout the grid. No agglomerated iron oxide species was observed independently, suggesting that the impregnation occurred mostly inside the mesopores. Noticeable high angle reflections (shown in the inset of figure 1 for

Table 1. Physico-chemical characterization of iron-loaded mesoporous silica.

No.	Fe loading[1]	BET surface area (m^2 g^{-1})	Pore diameter (Å)	Pore volume (cc g^{-1})
1	–	1080	39.2	0.84
2	2.70	567	32.1	0.53
3	2.95	512	32.5	0.42
4	3.40	376	35.6	0.21

[1]Wt% of iron in the composite material.

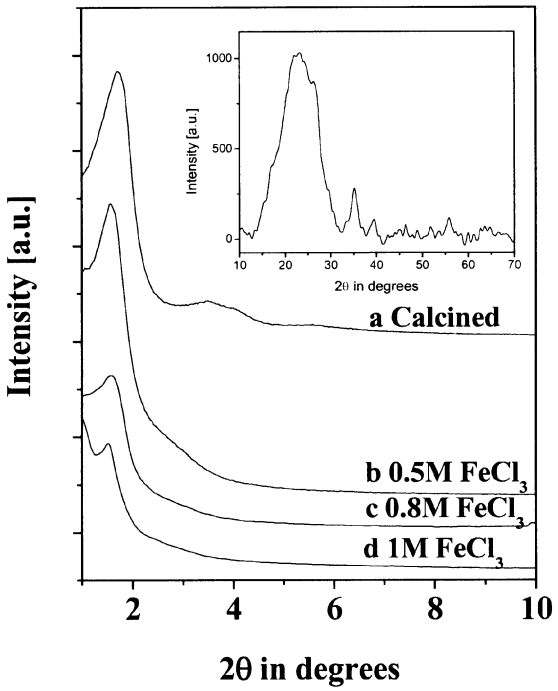

Figure 1. XRD patterns of mesoporous support MCM-41 (curve a, sample 1) before iron loading and Fe_2O_3 embedded mesoporous silica samples 2 (curve b, 0.5 M $FeCl_3$), 3 (curve c, 0.8 M $FeCl_3$) and 4 (curve d, 1 M 0.5 M $FeCl_3$). High angle diffraction pattern of sample 2 is shown in the inset.

sample 2) in the XRD patterns of these iron-loaded samples suggested the presence of nanoclustered α-Fe_2O_3 [9] inside the 2D hexagonal mesopore. Sample 4 with highest iron loading showed poorly ordered diffraction peak (curve d in figure 1).

In figure 3, N_2 adsorption/desorption isotherms for iron-loaded mesoporous silica (sample 2, curve a) as well as mesoporous silica host (sample 1, curve b) are shown. Pore size distributions for these samples are shown in the inset. Isotherms, as shown in figure 3 were type IV [7,20] in nature. As shown in figure 3, pore size distribution which was quite narrow before iron loading, becomes quite broad with a considerable reduction of pore diameter for sample 2. For other samples also similar decrease in pore diameter, pore volume and surface area was observed (table 1). Average pore diameter for this iron-loaded mesoporous silica sample employing BJH model was 2.6–3.2 nm [7,20]. The BET surface areas of samples 2 and 3 were moderate considering moderate concentration of iron and impregnation condition. These data are due to the reduction of mesopore diameter and BET surface area after the impregnation of iron oxide nanoparticles suggested the deposition of iron oxide clusters inside mesopores. Pore diameter and d spacing measured from TEM image analysis agreed well with these experimental data obtained from XRD and N_2 sorption.

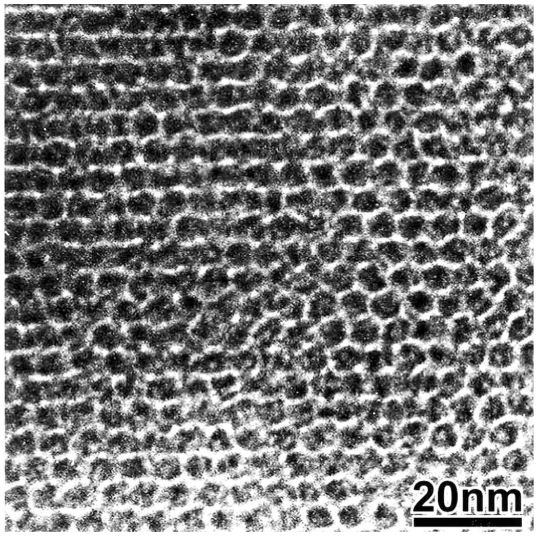

Figure 2. TEM image of Fe_2O_3 nanoparticles in the mesoporous silica (sample 2).

In figure 4, UV–visible diffuse reflectance spectrum of iron-loaded mesoporous silica (curve b, sample 2, representative) is shown. Samples 3 and 4 also showed almost similar behavior. Corresponding spectrum for bulk Fe_2O_3 is given in curve c for comparison. This bulk α-Fe_2O_3 showed a broad adsorption band in 320–670 nm wavelength with absorption maxima at 500 nm. The UV–visible spectra of the mesoporous ferrisilicate materials showed a very strong absorption band in the 200–330 nm wavelength with maxima at *ca.* 219 and 255 nm (figure 4a, [8]). This high-energy absorption band associated with ligand to metal charge transfer (LMCT) is the characteristic of isolated tetrahedral coordination of Fe^{3+} and has been also observed for mesoporous FeS-1 [21]. These two bands have been assigned to electronic transition of O^{2-} to the t_{2g} and e_g orbitals of Fe^{3+} in the iron oxide cluster. However, the absorption band of the iron-loaded mesoporous composite material (figure 4, curve b) is quite different from the mesoporous ferrisilicate material and showed four absorption maxima at 212, 262, 356 and 494 nm. Later, two absorptions were also observed for the bulk α-Fe_2O_3 sample. This could be explained by the quantum size effect [1] in UV absorption. Identification of the oxidation state and nature of iron species in the nanocomposite material [22] is essential in determining its microstructure. UV–visible data suggested that the loading of iron have very little effect on the oxidation state of these materials and in almost all cases Fe(III) was the oxidation state of iron. The presence of α-Fe_2O_3 phase suggested the hexa-coordination of iron in the nanocomposite materials. Fe_2O_3 nanoparticles with different sizes were investigated using Fe K-edge X-ray absorption near-edge structure [23] recently, which suggested mostly Fe sites with octahedral or distorted octahedral coordination. Experimental results thus explained the formation of iron oxide species having aggregates inside the channels of the mesopores.

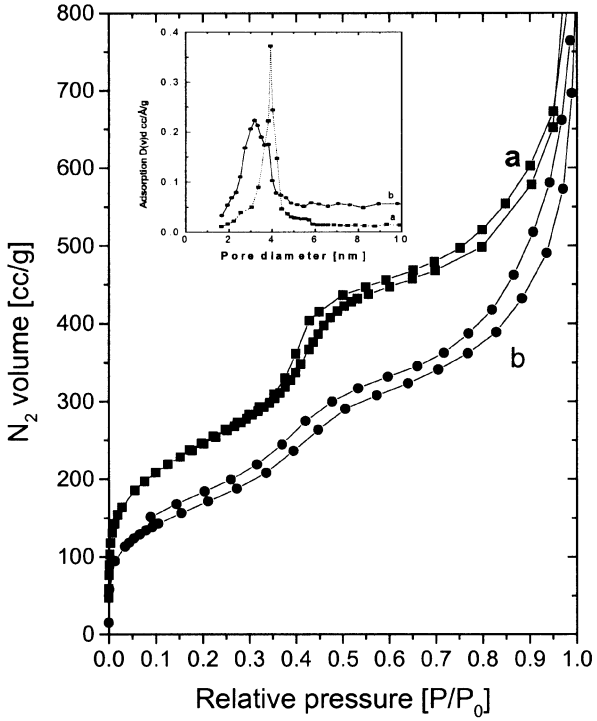

Figure 3. N_2 adsorption/desorption isotherms of mesoporous MCM-41 (curve a) and sample 2 (curve b) after iron loading. BJH pore size distributions are shown in the inset.

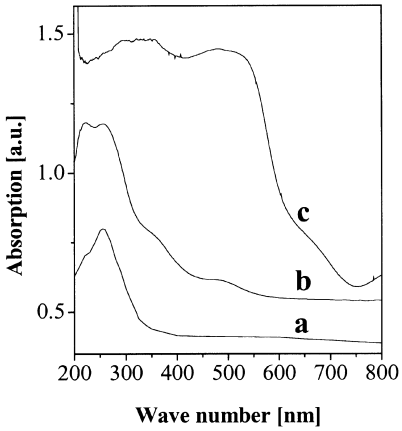

Figure 4. UV–visible diffuse reflectance spectra of surfactant free Fe-MCM-41 (curve a), Fe_2O_3 embedded mesoporous silica (curve b, sample 2) and bulk Fe_2O_3 (curve c).

4. Conclusions

α-Fe_2O_3 nanoparticles have been successfully encapsulated inside the mesopores of MCM-41 silica. Ordered mesophases were observed till the highest loading of iron was achieved (2.95 wt% with respect to SiO_2) in these mesoporous materials. Beyond this loading limit disordered mesophases were obtained. UV–visible spectra suggested octahedral/distorted octahedral coordination of Fe^{3+} in the iron oxide clusters. The impregnated Fe_2O_3 forms well-dispersed isolated iron oxide clusters inside the 2D-hexagonal channels of mesoporous silica host. From the experimental results it can be concluded that the inorganic mesoporous silica in the pore wall directs a physical constraint necessary to prevent the creation of large Fe_2O_3 agglomerates and enables the formation of nanosized Fe_2O_3 clusters inside the uniform mesopores.

Acknowledgement

This work was partly supported by NanoScience and Technology Initiative (NSTI) and Fast Track YS (grant number SR/FTP/CS-24/2001) projects of the Department of Science and Technology (grant number SR/FTP/CS-24/2001) and Council of Scientific and Industrial Research (grant number 01(1800)/02/EMR-II), New Delhi.

References

[1] V L Colvin, M C Schlamp and A P Alivisatos, *Nature (London)* **370**, 354 (1994)
[2] S Sun, C B Murray, D Weller, L Folks and A Moser, *Science* **287**, 1989 (2000)
[3] S M Ponder, J G Darab, J Bucher, D Caulder, I M Craig, L Davis, N M Edelstein, W Lukens, H Nitsche, L Rao, D K Shuh and T E Mallouk, *Chem. Mater.* **13**, 479 (2001)
[4] M Allen, D Willits, J Mosolf, M Young and T Douglas, *Adv. Mater.* **14**, 1562 (2002)
[5] D Beydoun, R Amal, G Low and S Mcevoy, *J. Nanoparticle Res.* **1**, 439 (1999)
[6] T Fried, G Shemer and G Markovich, *Adv. Mater.* **13**, 1158 (2001)
[7] C T Kresge, M E Leonowicz, W J L Roth, J C Vartuli and J S Beck, *Nature (London)* **359**, 710 (1992)
[8] S Samanta, S Giri, P U Sastry, N K Mal, A Manna and A Bhaumik, *Ind. Eng. Chem. Res.* **42**, 3012 (2003)
[9] S Giri, S Samanta, S Maji, S Ganguli and A Bhaumik, *J. Magn. Magn. Mater.* **285**, 296 (2005)
[10] T Abe, Y Tachibana, T Uematsu and M Iwamoto, *J. Chem. Soc. Chem. Commun.* 1617 (1995)
[11] C Weiping and Z Lide, *J. Phys.: Condens. Matter* **9**, 7257 (1997)
[12] A J Rondinone, A C S Samia and Z J Zhang, *J. Phys. Chem.* **103**, 6876 (1999)
[13] S H Joo, S J Choi, I Oh, J Kwak, Z Liu, O Terasaki and R Ryoo, *Nature (London)* **412**, 169 (2001)
[14] C Minchev, R Köhn, T Tsoncheva, M Dimitrov, I Mitov, D Paneva, H Huwe and M Fröba, *Stud. Surf. Sci. Catal.* **142**, 1245 (2002)

[15] H Guo, W Xu, M-H Cui, N-L Yang and D L Akins, *Chem. Commun.* 1432 (2003)
[16] K Shafi, A Ulman, A Yan, N L Yang, C Estournes, H White and M H Rafailovich, *Langmuir* **17**, 5093 (2001)
[17] T Hirai, T Saito and I Komasawa, *J. Phys. Chem.* **B105**, 9711 (2001)
[18] C Cannas, G Concas, D Gatteschi, A Falqui, A Musinu, G Piccaluga, C Sangregorio and G Spano, *Phys. Chem. Chem. Phys.* **3**, 832 (2001)
[19] X Wu and S-B Kim, *Elec. Solid-State Lett.* **2**, 184 (1999)
[20] S J Gregg and K S W Sing, *Adsorption, surface area and porosity* (Academic, New York, 1992) p. 49
[21] A Tuel, I Arcon and J M M Millet, *J. Chem. Soc. Faraday Trans.* **94**, 3501 (1998)
[22] S Morup and E Tronc, *Phys. Rev. Lett.* **72**, 3278 (1994)
[23] L X Chen, T Liu, M C Thurnauer, R Csencsits and T Rajh, *J. Phys. Chem.* **B106**, 8539 (2002)
[24] A Bhaumik, S Samanta, N K Mal, P Kumar and A Manna, *Chem. Eng. Sci.* **60**, 839 (2005)